A cell wall-associated gene network shapes leaf boundary domains

Nathalie Bouré, Alexis Peaucelle, Magali Goussot, Bernard Adroher, Ludivine Soubigou-Taconnat, Néro Borrega, Eric Biot, Zakia Tariq, Marie-Laure Martin-Magniette, Véronique Pautot, et al.

© 2022. Published by The Company of Biologists Ltd | Development (2022) 149, dev200359. doi:10.1242/dev.200359

RESEARCH ARTICLE

A cell wall-associated gene network shapes leaf boundary domains

Nathalie Bouré[1,2], Alexis Peaucelle[1], Magali Goussot[1], Bernard Adroher[1], Ludivine Soubigou-Taconnat[3,4], Néro Borrega[1], Eric Biot[1], Zakia Tariq[3,4], Marie-Laure Martin-Magniette[3,4], Véronique Pautot[1], Patrick Laufs[1] and Nicolas Arnaud[1,*]

ABSTRACT

Boundary domains delimit and organize organ growth throughout plant development almost relentlessly, building plant architecture and morphogenesis. Boundary domains display reduced growth and orchestrate development of adjacent tissues in a non-cell-autonomous manner. How these two functions are achieved remains elusive despite the identification of several boundary-specific genes. Here, we show using morphometrics at the organ and cellular levels that leaf boundary domain development requires SPINDLY (SPY), an O-fucosyltransferase, to act as cell growth repressor. Furthermore, we show that SPY acts redundantly with the CUP-SHAPED COTYLEDON transcription factors (CUC2 and CUC3), which are major determinants of boundaries development. Accordingly, at the molecular level CUC2 and SPY repress a common set of genes involved in cell wall loosening, providing a molecular framework for the growth repression associated with boundary domains. Atomic force microscopy confirmed that young leaf boundary domain cells have stiffer cell walls than marginal outgrowth. This differential cell wall stiffness was reduced in *spy* mutant plants. Taken together, our data reveal a concealed *CUC2* cell wall-associated gene network linking tissue patterning with cell growth and mechanics.

KEY WORDS: *Arabidopsis*, Boundaries, Morphogenesis, Growth

INTRODUCTION

Boundaries act both as frontiers to separate adjacent tissues or organs and as organizing centers providing positional clues to control the fate of neighboring cells (Dahmann et al., 2011; Irvine and Rauskolb, 2001). Thus, boundary domains are required to pattern developing organs correctly. For instance, in animals defects in boundaries lead to developmental abnormalities, including impaired wing or brain development (Dahmann et al., 2011). In contrast with the determinate development occurring in animals, plants continuously form new aerial growth axes separated from the shoot apical meristem (SAM) to build their architecture. These new growth axes can either produce new branches or give rise to specialized lateral organs, such as leaves or flowers. Independently of their fate, all lateral organs are separated from the meristem by boundary domains, which delimitate cell territories and orchestrate their development (Aida and Tasaka, 2006). Despite decades of efforts to decipher their functions, plant boundary domains remain an elusive population of cells for which little information is available.

The patterning and maintenance of boundary domains rely on the activity of the CUP-SHAPED COTYLEDON (CUC) transcription factors, which belong to the NAC transcription factor family (Aida et al., 1997; Vroemen et al., 2003). There are three CUC genes in *Arabidopsis*: *CUC1*, *CUC2* and *CUC3*. *CUC1* and *CUC*2 mRNA but not *CUC3* are targeted by the microRNA *MIR164* (Laufs et al., 2004). The CUC transcription factors regulate both shoot meristem formation (Aida et al., 1999) and correct organ separation in various developmental contexts (Aida et al., 1997; Burian et al., 2015; Gonçalves et al., 2015). Accordingly, CUC2 and CUC3 are key regulators of leaf shape through their roles on leaf margin development (Blein et al., 2008; Hasson et al., 2011; Nikovics et al., 2006), *CUC1* being not expressed during leaf development (Nikovics et al., 2006). During leaf development, CUC2 and CUC3 define boundary domains at the leaf margin – called sinuses – allowing differential growth to shape the leaf. At the cellular level, the coordinated activity of CUC2/3 transcription factors suppresses growth locally and has a positive effect at a distance on the initiation and maintenance of high growth rate probably via a mechanism involving auxin (Bilsborough et al., 2011). The CUC2 transcription factor acts through the activation of *CUC3* and *KLU* (also known as *CYP78A5*), encoding a cytochrome P450, which serves as a molecular relay, and through modulation of auxin signaling pathway (Maugarny-Calès et al., 2019). Acting downstream of *CUC2*, *CUC3* maintains reduced growth of the boundary domains via the control of cell growth through unknown molecular mechanisms (Serra and Perrot-rechenmann, 2020). Accordingly, *cuc2* loss-of-function mutants fail to initiate teeth and in *cuc3* loss-of-function mutants teeth growth is not maintained (Hasson et al., 2011). Several hormonal pathways impinge on boundary domain establishment (Hepworth and Pautot, 2015). For instance, brassinosteroids (BRs) have been shown to antagonize boundary domain formation through the downregulation of CUC genes (Gendron et al., 2012). Low BR levels are maintained within boundary domains by the activation of BAS1, a cytochrome P450 involved in BR catabolism, thus leading to the reduced growth of boundary domains (Bell et al., 2012). Auxin also plays a fundamental role during boundary domain establishment, exemplified by its implication in leaf serration development (Bilsborough et al., 2011). Other regulatory molecules have recently emerged as important regulators of boundary domains. The EPF/EPFL secreted peptides and the ERECTA family receptors

[1]Université Paris-Saclay, INRAE, AgroParisTech, Institut Jean-Pierre Bourgin (IJPB), 78000 Versailles, France. [2]Université Paris-Saclay, 91405 Orsay, France. [3]Université Paris-Saclay, CNRS, INRAE, Univ Evry, Institute of Plant Sciences Paris-Saclay (IPS2), 91405 Orsay, France. [4]Université de Paris, CNRS, INRAE, Institute of Plant Sciences Paris-Saclay (IPS2), 91405 Orsay, France.

*Author for correspondence (nicolas.arnaud@inrae.fr)

V.P., 0000-0002-0059-0050; P.L., 0000-0003-4459-3445; N.A., 0000-0001-8571-5862

Handling Editor: Ykä Helariutta
Received 15 November 2021; Accepted 29 April 2022

Development (2022) 149, dev200359. doi:10.1242/dev.200359

contribute to boundary domain formation both during leaf development and ovule initiation, probably through modulation of auxin responses (Kawamoto et al., 2020; Kosentka et al., 2019; Tameshige et al., 2016).

In an attempt to identify new actors of boundary domains, we previously performed a genetic suppressor screen of a line overexpressing *CUC2* and identified *MUR1*, coding for a GDP-D-mannose 4,6-dehydratase involved in GDP-L-fucose production. More specifically, we showed that L-fucose contributes to boundary domain establishment in various developmental contexts (Gonçalves et al., 2017). Fucose is a hexose incorporated into xyloglucans, rhamnogalacturonan II and arabinogalactans in plant cell walls (O'Neill et al., 2001; Van Hengel and Roberts, 2002) and added to proteins through the activity of specific fucosyltransferases (Strasser, 2016).

Recently, SPINDLY (SPY) has been described as a O-fucosyltransferase able to target REPRESSOR OF GA (RGA), a negative regulator of the gibberellin (GA) signaling pathway from the DELLA family (Zentella et al., 2017), as well as PSEUDO-RESPONSE REGULATOR 5 (PRR5), a core circadian clock component (Wang et al., 2020). *spy* loss-of-function mutants were originally identified in a genetic screen for plantlet resistant to the GA biosynthesis inhibitor paclobutrazol (Jacobsen and Olszewski, 1993). This mutant displays constitutive GA phenotypes, suggesting that SPY negatively regulates the GA signaling pathway (Jacobsen et al., 1996). The implication that SPY may directly O-fucosylate RGA provides a molecular framework for the function of SPY in the GA signaling pathway. However, as *spy* mutants do not completely resemble wild-type (WT) plants treated with GA (Swain et al., 2001), it is likely that SPY also acts through GA-independent pathways. This has been recently shown during root development where SPY regulates root hair patterning in a GA-independent pathway (Mutanwad et al., 2020). Accordingly, SPY has been proposed to positively regulate cytokinin (CK) signaling, highlighting a central role in the regulation of GA/CK crosstalk throughout plant development (Greenboim-Wainberg et al., 2005). This GA/CK hormonal crosstalk is instrumental in the maintenance of *KNOX* (Class I *KNOTTED1*-like homeobox)-dependent meristematic activity (Hay et al., 2002; Jasinski et al., 2005), which implies that SPY has a crucial role during SAM development and/or maintenance. In addition to this function in the SAM, several reports show that *spy* mutants have altered leaf development with little or no serrations at their margins (Greenboim-Wainberg et al., 2005; Maymon et al., 2009), but detailed analysis of the function of SPY in these boundary domains development is lacking.

Here, we investigated the role of SPY in leaf development. SPY is required to maintain restricted growth of the sinus cells. Furthermore, our genetic analysis suggests that *SPY* acts redundantly with *CUC2* and *CUC3* to control boundary domain development. At the molecular level, both SPY and CUC2 regulate a common set of genes controlling cell wall properties. Accordingly, we show that CUC2 represses cell growth independently of CUC3, possibly via modifications of cell wall mechanics. Together, these data provide a molecular framework for the role of SPY during boundary domain development whereby SPY and CUC2 act through a common pathway, and reveal a concealed growth repressive function for CUC2 involving cell expansion.

RESULTS

SPY regulates leaf morphogenesis

Several *spy* mutant alleles (Greenboim-Wainberg et al., 2005; Maymon et al., 2009; Steiner et al., 2012) have been reported to result in leaves with little or no serration, but this leaf phenotype was never fully characterized. Therefore, we quantified the leaf shape of the loss-of-function *spy-3* mutant. The *spy-3* mutant contains a G>A transition changing a glycine to a serine residue at position 593 of the SPY protein, resulting in a non-functional protein (Jacobsen et al., 1996) (Fig. S1). *spy-3* mutant and WT mature leaves displayed similar blade lengths but their widths, and hence their blade area, were smaller in *spy-3* (Fig. S2A-C). Both morphometrics and dissection index (DI) calculations, global descriptors of leaf complexity (Gonçalves et al., 2017), showed that *spy-3* leaves are smoother than WT leaves (Fig. 1A-C). To investigate further, we measured the shape of the second tooth (as the ratio between tooth height and tooth width) in this dataset, revealing that WT serrations are pointier than *spy-3* serrations (Fig. 1D). Two additional alleles, namely *spy-22* and *spy-23* (Figs S1 and S3), had smoother leaves than the WT with less-pronounced serrations, ruling out the possibility of *spy-3*-specific bias on leaf morphology. Furthermore, a *spy-22* mutant expressing the *pSPY::SPY-FLAG* construct had a restored WT leaf shape phenotype (Fig. S3). Taken together, our results show that *SPY* is involved in the development of leaf serrations.

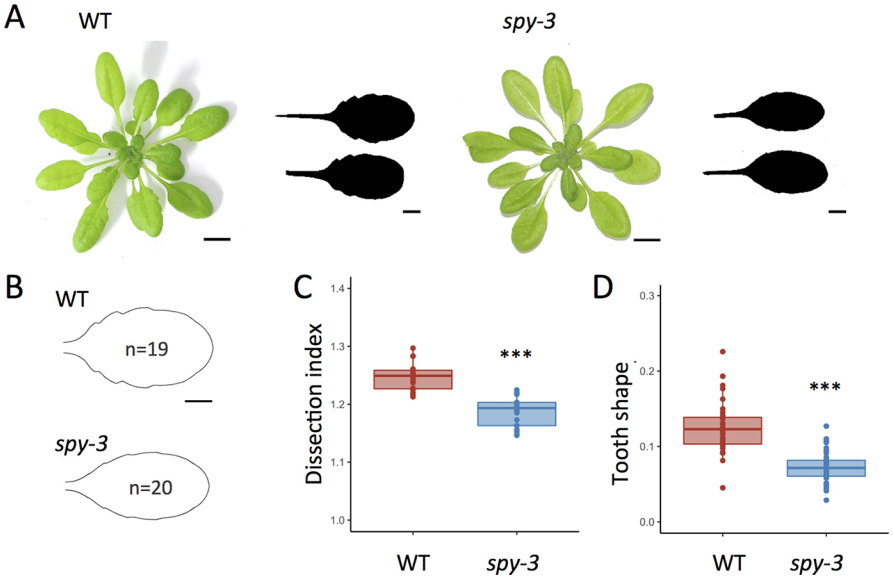

Fig. 1. Morphometric analysis of *spy-3* mature leaf shape. (A) WT and *spy-3* mutant rosette from plants grown in short-day conditions for 6 weeks. Representative silhouettes from mature leaves from ranks 11-13 are also represented. Scale bars: 1 cm. (B) Mean shape of mature leaves of WT and *spy-3* mutant. Scale bar: 1 cm. (C) Quantification of alpha-hull normalized dissection index for WT and *spy-3* mature leaves. (D) Quantification of the shape of the second tooth from WT and *spy-3* mature leaves. (B-D) WT (n=19) and spy-3 (n=20) 6-week-old leaves grown in short-day conditions, ranks 11-13. ***P<0.0001 (one-tailed unpaired Student's t-test).

Development (2022) 149, dev200359. doi:10.1242/dev.200359

SPY is required for growth serration maintenance

As mature leaf shape results from the sum of processes occurring at different developmental times, it is important to access growth kinetic data of the *spindly* mutant to conclude about the precise roles of SPY during leaf shape development. To do this, we reconstructed detailed developmental trajectories of *spy-3* loss-of-function mutant leaves using MorphoLeaf software from a set of leaves from ranks 11, 12 and 13. As both the leaf initiation rate and the leaf growth rates are comparable between *spy-3* and the WT up to 6 mm length (Fig. S4), we chose to limit our morphometric analysis to this early stage and use leaf blade length as a proxy for leaf developmental stage. Tooth 1 height was drastically reduced in *spy-3* from early stages and never reached WT values (Fig. 2A), whereas tooth 1 width was not modified at early developmental stages (up to 3 mm) (Fig. 2B), resulting in sharper teeth in the WT (Fig. 2C). Together, our data suggest that SPY is involved in teeth growth maintenance. As maintenance of tooth growth is associated with the definition of the leaf boundary domain at the sinus (Hasson et al., 2011; Maugarny-Calès et al., 2019), we analyzed sinus angle as a local parameter related to local growth repression at the sinus. Although the evolution of the sinus angle for the distal sinus of tooth 1 throughout its development had comparable dynamics both in *spy-3* and in WT, the *spy-3* sinus angle was always less pronounced than the WT sinus angle (Fig. 2D). These data suggest that the alteration of leaf shape may partially result from local defects in boundary domain definition in the *spy-3* mutant.

SPY is required to inhibit sinus cell growth during leaf development

During leaf development, spatial differences in cell growth rate sustain tooth outgrowths (Serra and Perrot-rechenmann, 2020), which are integrated at the leaf level leading to final leaf shape. As sinus angle was altered in the *spy-3* mutant compared with the WT, we set out to analyze the sinus at the cellular level. The distribution of cell surface in 3D acquisitions for tooth 1 of leaves from ranks 11, 12 and 13 was hence measured in both genotypes (Fig. 2E). We focused on the first distal sinus to limit bias due to the mechanical constraints of the previous tooth outgrowth. The shape of the tooth and the depth of the sinus were different between *spy-3* and WT in these 3D acquisitions, which confirmed the data from the 2D developmental kinetics. In order to assess the size of the sinus cells specifically, we analyzed the Gaussian curvature of the 3D projected surface. Sinuses were identified as surface areas that exhibited a negative Gaussian curvature (Fig. S5) (Serra and Perrot-rechenmann, 2020) and the surfaces of sinus-specific cells were measured from independent leaves. Sinus cell surfaces were then plotted according to tooth width for both *spy-3* and WT leaves (Fig. 2F). For teeth 1 up to 150 µm wide, sinus cell sizes of early leaf primordia were not significantly different between *spy-3* and the WT. Later, for teeth ranging from 150 to 250 µm and 250 to 500 µm, sinuses of *spy-3* mutant leaves were composed of larger cells than those in WT. Our data show that SPY is required to maintain restricted sinus cell growth at late stages of tooth development. Interestingly, the *cuc3-105* loss-of-function mutant has been described to have bigger cells at the sinus due to local release of cell growth (Serra and Perrot-rechenmann, 2020). Thus, *spy-3* and *cuc3-105* mutants display very similar sinus cell phenotypes, suggesting that SPY and CUC transcription factors have similar roles in sinus cell development. This leads to the question of whether they function through a common pathway to coordinate growth restriction of sinus cells.

SPY, CUC2 and CUC3 act redundantly during boundary domain development

To check whether SPY acts in a CUC-dependent pathway to define boundaries, we first analyzed CUC/SPY genetic interactions using *CUC2g-m4*, a mutated version of *CUC2* with altered *MIR164*-target site, leading to a local overexpression of *CUC2* mRNA and very serrated leaves (Maugarny-Calès et al., 2019; Nikovics et al., 2006). *CUC3*, which acts downstream of *CUC2*, has already been shown to reduce leaf serration of the *CUC2g-m4* line (Hasson et al., 2011). CUC2 overexpression leaf phenotypes (measured by DI calculations) were suppressed in *spy-3* and *cuc3-105* backgrounds (Fig. 3A). Furthermore, we used the *mir164a* loss-of-function mutant as an alternative way of increasing *CUC2* levels and found that the over-serrated leaf phenotype of *mir164a* was suppressed by the *spy-3* mutation (Fig. 3A). Together, these genetic data suggest that CUC2 requires SPY or CUC3 activity to control leaf serration development.

Given that *spy3* and *cuc3-105* mutants have very similar phenotypes both at the organ and at the cellular scales, and that they both suppress the CUC2 highly serrated leaves phenotype, we hypothesize that *CUC3* and *SPY* act in the same genetic pathway to control serration development. To test this idea, we generated a double *spy3 cuc3-105* mutant and analyzed its leaf developmental trajectory (Fig. 3B). As CUC3 maintains tooth growth by locally inhibiting the growth of sinus cells, we used tooth height of the first tooth as a proxy of CUC3 activity. Strikingly, when the tooth height of the first tooth was measured for different tooth width classes, *cuc3-105* and *spy-3* displayed comparable quantitative phenotypes, whereas the two mutations together had an additive effect on tooth height, suggesting that they act independently on leaf shape (Fig. 3B). Accordingly, *spy-3* and *cuc3-105* mutations also had an additive effect on the over-serrated *CUC2gm-4* phenotype (Fig. 3A). These data imply that alternative routes exist to restrict growth at the sinus independently of *CUC3*. In order to decipher the relative contribution of *SPY*, *CUC2* and *CUC3* to boundary cell growth, we decided to analyze their roles during cotyledon rather than during leaf development because no serrations are initiated when CUC2 activity is altered. Both double mutants *spy-3 cuc3-105* and *spy-3 cuc2-1* showed stronger cotyledon fusion phenotypes compared with the corresponding simple mutants showing that SPY acts redundantly with CUC2 and CUC3 to define boundaries (Table 1, Fig. S6). This result indicates that SPY acts in different developmental contexts and suggests that SPY contributes more generally to the definition of developmental boundary domains.

SPY and *CUC2* act through a common molecular network to restrict sinus cell growth

Our genetic analysis suggests that *CUC2*, *CUC3* and *SPY* redundantly restrict boundary domain growth. As we saw a local growth defect in the *spy-3* mutant, we first tested whether *SPY* was expressed together with the CUC genes within the leaf boundary domains. We used the *pSPY::SPY-GFP* reporter line crossed with either *pCUC3::CFP* or *pCUC2::RFP* to monitor simultaneously *SPY* localization and CUC gene expression patterns. Although SPY is broadly expressed in leaf epidermis at early developmental stages, it overlapped with *CUC2* and *CUC3* within leaf boundary domain cells (Fig. S7). In addition, we show that even though *CUC2* levels vary greatly between *cuc2-1* mutant, the WT and the *CUC2gm-4* line, the expression levels of *SPY* do not change, suggesting that SPY expression is not regulated by CUC2 (Fig. S8).

As our genetic analysis shows that CUC2 activity requires *SPY*, we next investigated how this translates at the molecular level.

Development (2022) 149, dev200359. doi:10.1242/dev.200359

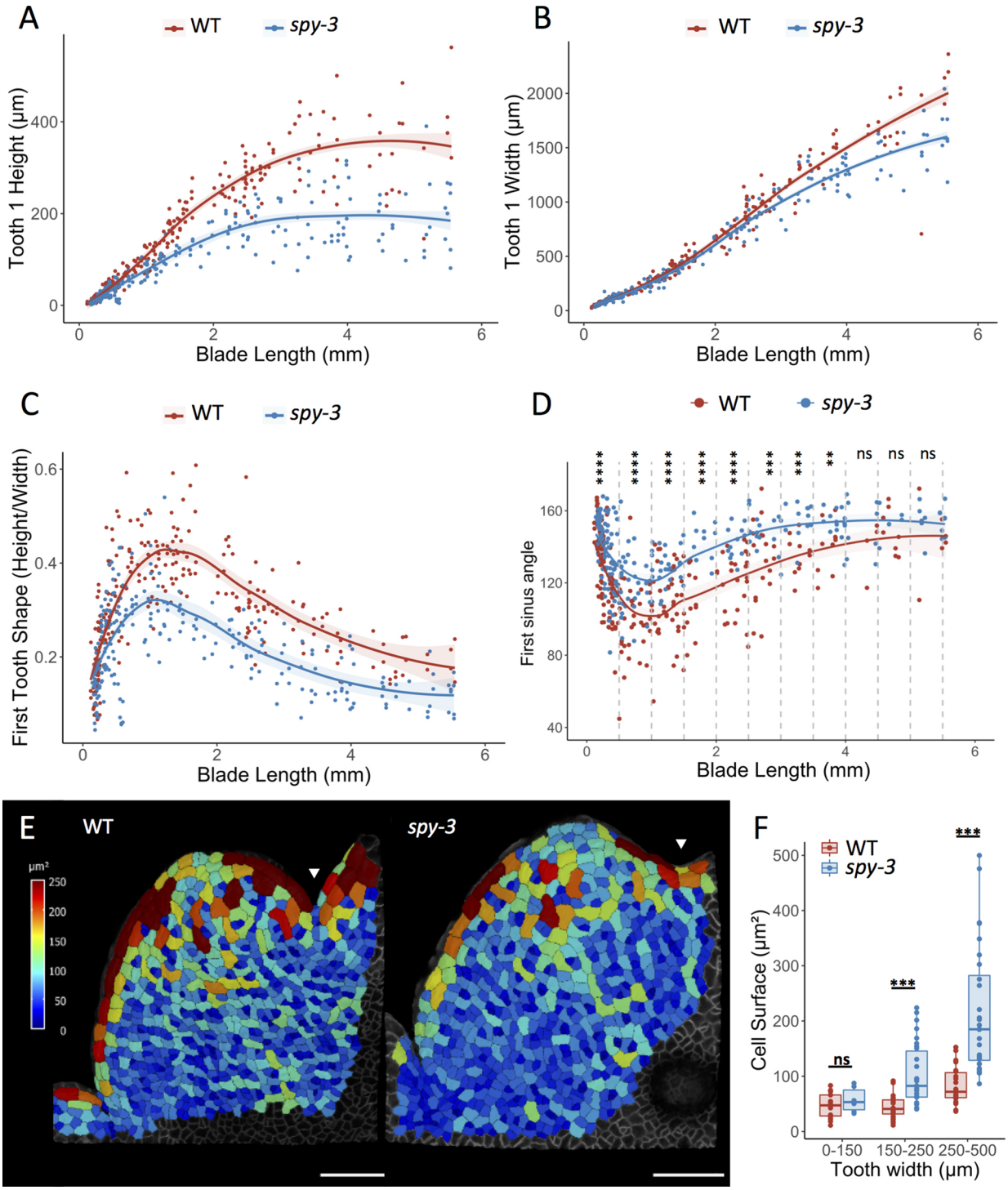

Fig. 2. Developmental kinetics and cell size quantification during *spy-3* serration development. (A) First tooth height plotted against blade length for WT and *spy-3*. (B) First tooth width plotted against blade length for WT and *spy-3*. (C) Tooth shape of the first tooth, calculated as tooth height over tooth width plotted against blade length for WT and *spy-3*. (A-C) Leaf ranks 11-13 dissected at different stages of development from WT (n=190) and *spy-3* (n=194) plants grown in short-day conditions were used. Each tooth is represented by a dot, and a LOESS curve is shown for visual interpretation. (D) Mean first sinus angle measured in short-day-grown WT (n=190) and *spy-3* (n=194) and plotted against blade length. For statistical analysis, data were split into 250 µm-wide classes. **P<0.01, ***P<0.001, ****P<0.0001 (one-tailed unpaired Student's t-test). (E) Representative cell area heatmaps for WT and *spy-3* from the first tooth sinus cells. Arrowheads indicate the crease defining the first apical sinus on each tooth. Scale bars: 50 µm. (F) Projected surface quantification from the first tooth sinus cells plotted against tooth width. WT (n=17), *spy-3* (n=6) for 0-150 µm; WT (n=37), *spy-3* (n=30) for 150-250 µm; WT (n=22), *spy-3* (n=28) for 250-500 µm. ***P<0.001 (one-tailed unpaired Student's t-test). ns, not significant.

Previous transcriptomic analysis identified genes differentially expressed in *spy-3* compared with WT (Qin et al., 2020). To identify CUC2 downstream elements, we performed transcriptomic profiling on whole seedlings of an activated CUC2 dexamethasone (DEX)-inducible line. Among the differentially expressed genes, we found that about 20% of the genes that were upregulated in the

Development (2022) 149, dev200359. doi:10.1242/dev.200359

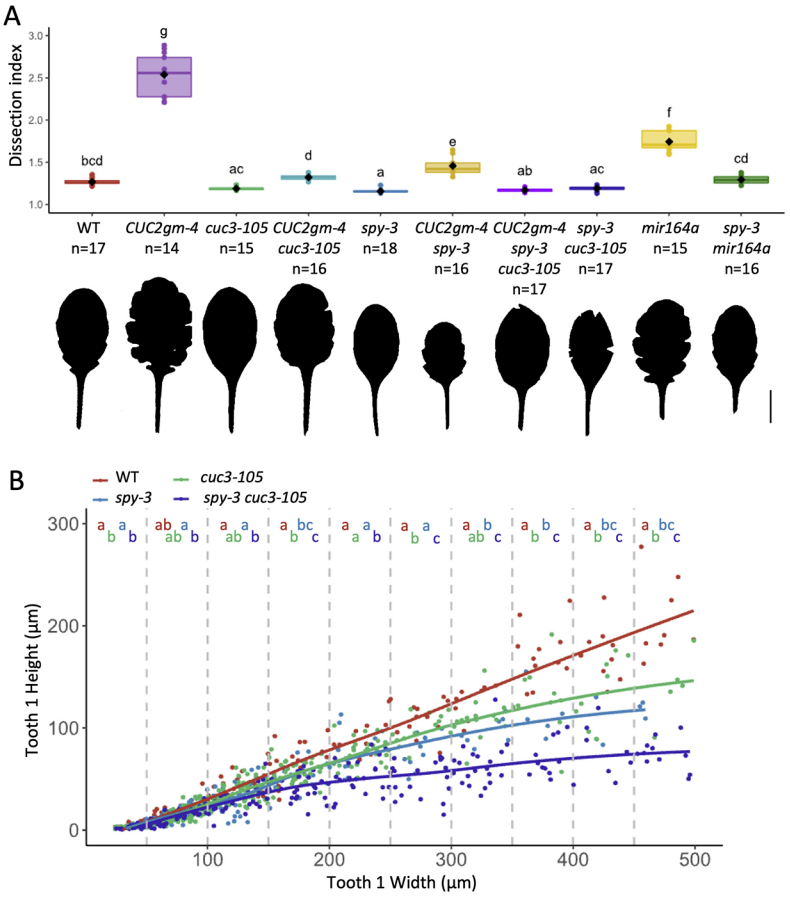

Fig. 3. *CUC* and *SPY* genetic interactions during leaf development. (A) Quantification of alpha-hull-normalized dissection index for WT (*n*=17), *CUC2g-m4* (*n*=14), *cuc3-105* (*n*=15), *CUC2g-m4 cuc3-105* (*n*=16), *spy-3* (*n*=18), *CUC2g-m4 spy-3* (*n*=16), *CUC2g-m4 spy-3 cuc3-105* (*n*=17), *spy-3 cuc3-105* (*n*=17), *mir164a* (*n*=15) and *spy-3 mir164a* (*n*=16) mature leaves of ranks 11-13. A representative leaf silhouette is shown for each genotype analyzed. Scale bar: 1 cm. (B) Analysis of *CUC3* and *SPY* genetic interactions during leaf development. First tooth height from WT (*n*=190), *spy-3* (*n*=194), *cuc3-105* (*n*=213) and *spy-3 cuc3-105* (*n*=191) plotted against 50 µm-wide first tooth width classes. Short-day-grown plants from 22 to 50 days after sowing were used. Different colored letters represent statistical significance in one-way ANOVA analysis performed within each class for every genotype (colored letters correspond to the genotype analyzed), followed by Tukey comparison test (P<0.05).

spy-3 mutant were downregulated upon CUC2 induction (Table S3). Indeed, we identified 2569 genes that were downregulated 6 h after *CUC2* induction (FDR<0.05) and, of these, 100 were upregulated in the *spy-3* mutant, which represents a significant proportion of the 493 genes upregulated in total in the *spy-3* mutant (hypergeometric test, P=6.06E−14) (Fig. 4A). Gene ontology analysis performed using this set of 100 genes revealed an enrichment in genes related to plant-type cell wall [GO:0009505, enrichment 9.65, raw P=4.31E−05 (Fisher exact test), FDR=4.45E−02] with a function related to cell wall organization and biogenesis [GO:0071554, enrichment 7.38, raw P=1.13E−06 (Fisher exact test), FDR=6.75E03]. Among these genes, we identified several genes coding for xyloglucan endotransglucosylase/hydrolases (XTH4, XTH15, XTH18 and XTH19), arabinogalactan proteins (AGP4, AGP7, AGP9 and AGP12), as well as two genes coding for expansin-like proteins (EXLA1 and EXLA2). These genes contribute to cell wall loosening. Indeed, XTH18 and XTH19 were both previously shown to be involved in the control of hypocotyl growth, as overexpressing lines for *XTH18* and *XTH19* both promoted hypocotyl growth in the dark (Miedes et al., 2013). In addition, AGP4, AGP7, AGP9 and AGP12 were identified in a large-scale gene expression pattern study on fast-growing seedlings as robust markers of growth (Kohnen et al., 2016). Similar observations for XTH proteins, *EXLA2* overexpression is able to increase growth in hypocotyls grown in the dark (Boron et al., 2015). In addition, a biomechanical analysis of an *EXLA2*-overexpressing line showed that cell wall resistance was decreased in the hypocotyl, suggesting that EXLA2 may modify the cell wall organization and composition (Boron et al., 2015).

Table 1. Quantification of cotyledon fusion defects in *cuc2-1*, *cuc3-105* and *spy-3* mutant combinations

	Phenotype				Total seedlings
Genotype	Normal (%)	Weak (%)	Mild (%)	Strong (%)	*n*
Col-0	99.37	0	0.63	0	315
cuc3-105	99.52	0	0	0.48	631
spy-3	100	0	0	0	317
spy-3 cuc3-105	82.79	4.66	10.39	2.17	645
cuc2-1	100	0	0	0	320
spy-3 cuc2-1	82.57	6.59	10.52	0.31	637

Importantly, we have independently measured mRNA levels within leaf margins using laser-assisted microdissection in both WT and the *CUC2gm-4* line followed by transcriptomic analysis by RNA sequencing (RNA-seq). Our data confirm, first, that the cell wall remodeling genes identified so far are expressed at the leaf margin of WT plants, and then, that among these genes, *AGP12*, *EXLA2*, *XTH18* and *XTH19* had significantly reduced mRNA levels in *CUC2gm-4* leaf margins (Table S1). Therefore, the combined analysis of our transcriptomic study suggests that cell wall-remodeling enzymes are the functional elements acting downstream of CUC2 and SPY.

CUC2 represses cell expansion independently of CUC3

To test whether *CUC2* overexpression does indeed inhibit cell expansion, we analyzed the effect of CUC2 ectopic activation upon DEX treatment during the elongation of hypocotyls grown in the dark, which results mostly from cell elongation rather than

Development (2022) 149, dev200359. doi:10.1242/dev.200359

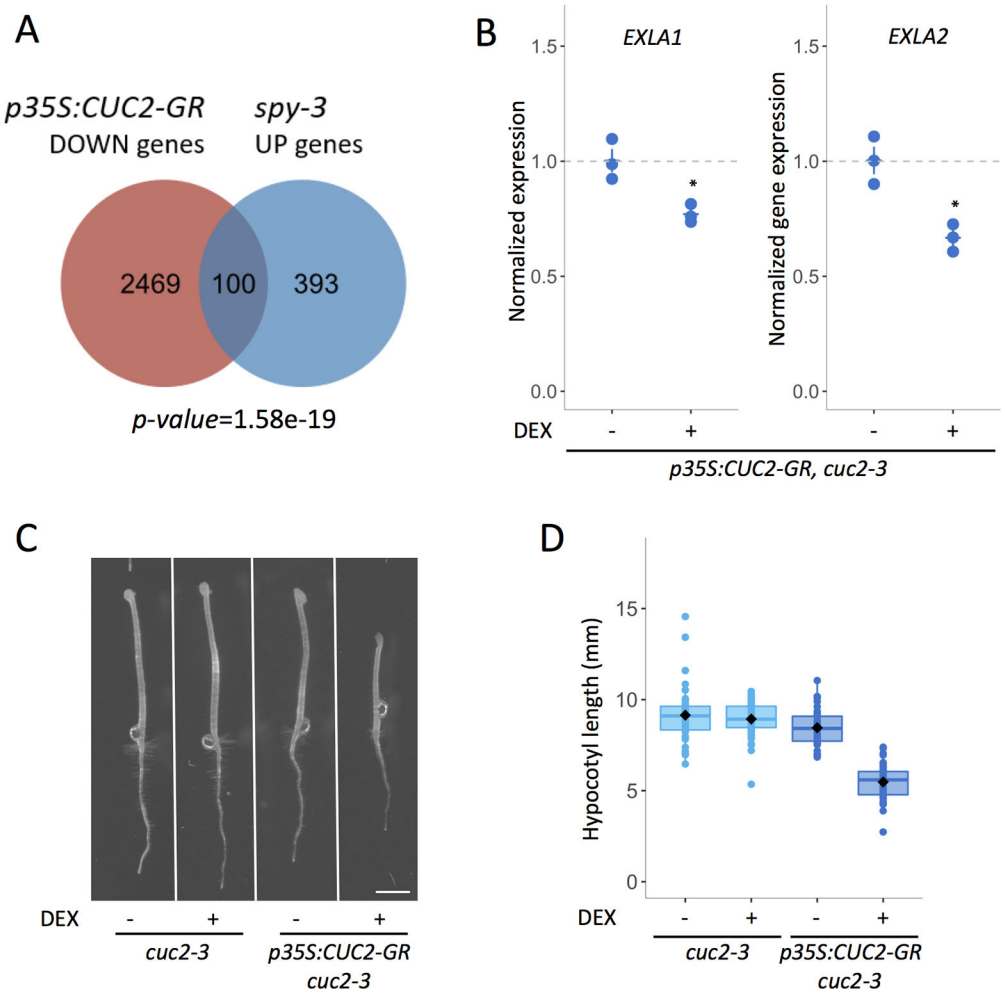

Fig. 4. CUC2 inhibition of dark-induced hypocotyl elongation is associated with downregulation of cell wall-relaxing genes. (A) A total of 2569 genes were downregulated in DEX-induced *p35S:CUC2-GR* line; 493 genes upregulated in *spy-3* mutant compared with WT were identified. *P*-value below the Venn diagram corresponds to hypergeometric probability ($N_{total\ At\ genes}$=33,602) (over-enrichment based on the cumulative distribution function of the hypergeometric distribution). (B) Expression level of *EXLA1* and *EXLA2* in a *p35S:CUC2-GR cuc2-3* line grown in the dark for 72 h *in vitro*, treated either with mock treatment or with 10 µM DEX. Each dot represents a biological RNA sample. *EXLA1* and *EXLA2* transcript levels were measured by real-time quantitative RT-PCR normalized to *EF1ALPHA* and *ACTIN 2*. **P*<0.05 (one-tailed unpaired Student's *t*-test). (C,D) Representative phenotypes (C) and corresponding hypocotyl length quantification (D) in *p35S:CUC2-GR cuc2-3* line and *cuc2-3* control grown in the dark for 72 h *in vitro*, treated either with mock treatment or with 10 µM DEX.

cell division (Gendreau et al., 1997). First, we independently validated that the expression level of *EXLA1* and *EXLA2*, two cell wall-remodeling genes, was inhibited upon CUC2 activation in this system model in accordance with our transcriptomic data (Fig. 4B). We then analyzed the effect of CUC2 activation on cell behavior and tissue phenotype. Under CUC-activation conditions, hypocotyls grown in the dark were significantly shorter and exhibited smaller hypocotyl epidermal cells compared with non-induced conditions (Fig. 4B,C). These results are in agreement with the reduced levels of expression of genes linked with cell wall plasticity after CUC2 induction. Taken together, our data suggest that overexpression of the transcription factor CUC2 is sufficient to repress a set of genes that have functions relating to cell wall loosening, providing a plausible molecular framework for the activity of CUC2.

The activity of CUC2 is mediated by CUC3, which acts as a molecular relay (Maugarny-Calès et al., 2019). As CUC2 and CUC3 redundantly control boundary domain development, it is possible that CUC2 alters cell elongation independently of CUC3. As no serrations are initiated in a *cuc2* loss-of-function mutant, this hypothesis has been difficult to test during leaf development. Here, we have the opportunity to test whether the CUC2-dependent growth repression function that we have highlighted with the DEX-induced CUC2 line in dark-grown hypocotyl depends on CUC3. When CUC2 is induced by DEX in absence of CUC3, dark-grown hypocotyls are shorter with smaller epidermal cells than those in non-induced conditions (Fig. 5A,B), showing that CUC2 acts independently of CUC3 on cell elongation in the dark-grown hypocotyl model. In order to check whether this reduction of growth is associated with changes in cell wall-related gene expression, we monitored their mRNA accumulation upon CUC2 induction in dark-grown hypocotyls. In a *cuc2-3 cuc3-105* mutant background, CUC2 induction is sufficient to drastically reduce the accumulation of *XTH18*, *XTH19*, *EXLA1* and *EXLA2* mRNA, showing that CUC2 inhibits their expression independently of *CUC3* (Fig. 5C). These results suggest that changes in cell wall gene expression triggered by CUC2 may counteract cell expansion.

Cell wall mechanics at the leaf margin

Our molecular data support a role for CUC2 in the control of cell wall properties. In order to check whether this is also the case in the organs where CUC2 is expressed, we used atomic force microscopy (AFM) to measure the cell wall stiffness of sinus cells (where *CUC2* is expressed) and compare with the cell wall stiffness of tooth cells (where *CUC2* is not expressed) (Fig. S9). In young leaf primordia, when the tooth starts to emerge, as shown by topographical images obtained using AFM, cells of the margins do not display different sizes between sinus and tooth domains in WT (Fig. 6A,B). Yet, sinus and tooth show a differential stiffness, cell sinus walls being stiffer than the cell tooth walls (Fig. 6A,B,E). This is consistent with both the expression pattern of *CUC2* and our molecular data showing that CUC2 inhibits the expression of genes known to promote cell wall loosening. To validate these data, we quantified the Apparent Young's modulus (*Ea*) to evaluate the elasticity of the

Development (2022) 149, dev200359. doi:10.1242/dev.200359

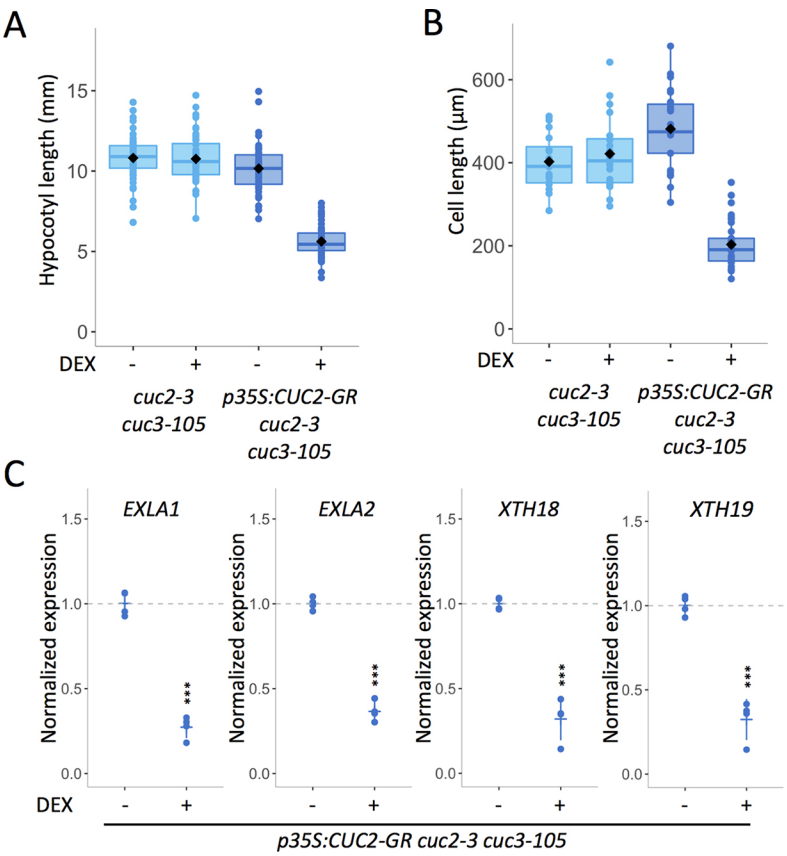

Fig. 5. CUC2 inhibits dark-induced cell elongation independently of CUC3. (A,B) Hypocotyl length quantification (A) and hypocotyl cell length quantification (B) in *p35S:CUC2-GR cuc2-3 cuc3-105* line and *cuc2-3 cuc3-105* control grown in the dark for 72 h *in vitro*, treated either with mock treatment or with 10 µM DEX. (C) Expression levels of *EXLA1*, *EXLA2*, *XTH18 and XTH19* in a *p35S:CUC2-GR cuc2-3* line grown in the dark for 72 h *in vitro*, treated either with mock treatment or with 10 µM DEX. Each dot represents a biological RNA sample. Transcript levels were measured by real-time quantitative RT-PCR normalized to *EF1ALPHA* and *ACTIN 2*. ***P<0.001 (one-tailed unpaired Student's *t*-test).

leaf margin tissue in another set of experiments analyzing cell wall stiffness in 12 young dissected leaves of the WT. This showed once again that sinus domains are consistently stiffer than tooth domains (Fig. 6F). As sinus and tooth definition trigger local topographical changes, it is possible that the changes in cell wall stiffness observed at the sinus may be reinforced by mechanical feedback. To test whether CUC2 can promote cell wall stiffness independently of topographical tissue changes, we ectopically expressed *CUC2* in dark-grown hypocotyls using the DEX-inducible *p35S:CUC2-GR* line. In this experiment, no tissue deformation occurred in the hypocotyl, but we still measured stiffer cell walls when CUC2 was overexpressed (Fig. S10), suggesting that CUC2 expression is sufficient to trigger changes in cell wall stiffness. Together, these results provide a mechanical framework for the development of boundary domains, which is in agreement with the quantitative description of leaf margin development in WT and observations in mutants harboring the null allele *cuc2-1*, in which local growth repression at the sinus preceding outgrowth of the tooth is specifically lost (Biot et al., 2016).

As CUC2 is required to initiate teeth, it is difficult to use *cuc2* loss of function to assess whether CUC2-dependent inhibition of cell expansion occurs also at the leaf margin. The *spy-3* mutant initiates teeth but their growth is not maintained owing to local cellular changes at the sinus during teeth development. *spy-3* therefore uncouples CUC2 functions as SPY leads to repression of the expression of a common set of genes with CUC2 that are related to the cell wall remodeling. We therefore used the *spy-3* mutant to check whether the reduced expression of cell wall genes acting downstream of CUC2 is sufficient to change the mechanical properties of the cell wall at the leaf margin. *spy-3* mutant young leaf primordia showed a reduction of the differential stiffness between tooth and sinus observed in the WT (Fig. 6C-E). We confirmed this by quantifying the Apparent Young's modulus (*Ea*) in another set of experiments analyzing cell wall stiffness in seven young *spy-3* dissected leaves (Fig. 6F). Although we highlight a significant difference between the sinus and tooth *Ea* values in *spy-3* leaves, differential stiffness was reduced compared with the sinus and tooth *Ea* values of the WT. These data support the idea that the set of genes commonly downregulated by CUC2 and SPY may impact cell wall stiffness at the leaf margin. Furthermore, it is important to note that stiffness changes precede the sinus cell morphological changes we observed in the *spy-3* mutant and occur at early stages of leaf development, thus providing a mechanical framework for the subsequent differential growth.

DISCUSSION

Plant development and architecture rely on the iterative production of lateral organs separated from the stem cell pool by boundary domains. Here, through the characterization of leaf margin phenotypes of *spy* mutants at multiple scales, we highlight a role for SPY in maintaining local growth repression of sinus cells redundantly with CUC transcription factors. Furthermore, we present evidence that SPY and CUC2 act through a common molecular network involving the reduction of the expression of genes associated with cell wall loosening. Accordingly, using hypocotyls grown in the dark together with a CUC2-inducible system, we show that CUC2 restricts cell expansion. This mode of action is supported by the fact that teeth and sinuses of young leaf primordia display differential cell wall stiffness: sinuses, where *CUC2* is expressed, show more rigid cell walls. Accordingly, cell wall stiffness is lower in the sinuses of *spy-3* leaves compared with the WT. Our data support a model whereby CUC2 can inhibit cell expansion independently of CUC3 acting through the repression of cell wall-relaxing genes.

Development (2022) 149, dev200359. doi:10.1242/dev.200359

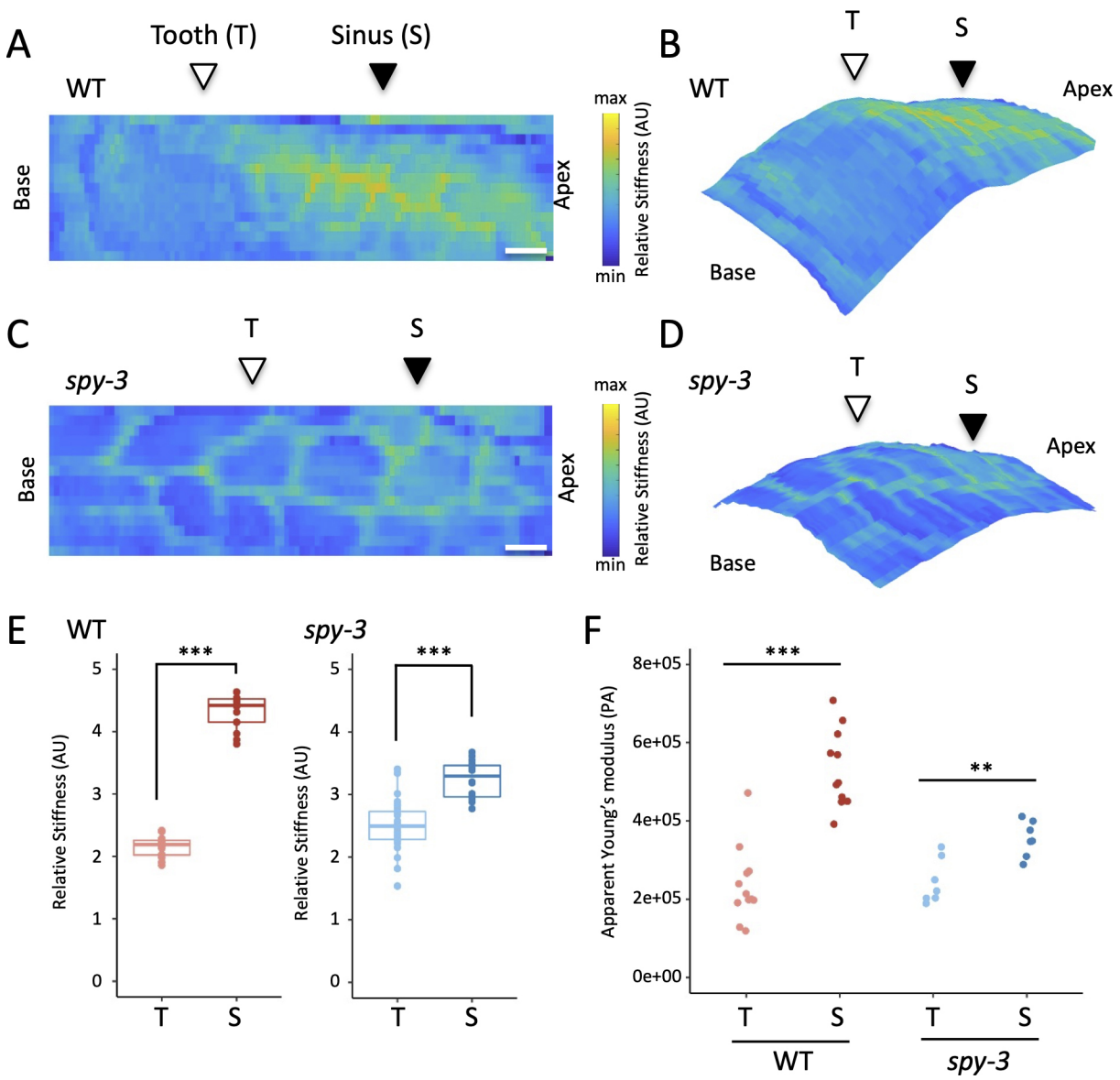

Fig. 6. Mechanics at the leaf margin of WT and *spy-3* mutant. (A,C) Representative maps of relative stiffness (arbitrary units, AU) measured on the middle domain of an approximately 150 µm-long growing primordium (rank 11) from WT (A) and *spy*-3 (C) plants grown in short-day conditions. Each pixel represents the relative stiffness calculated from a single force-indentation curve. Apico-basal polarity is indicated. Position of tooth (T) as well as sinus (S) are indicated. Scale bars: 10 µm. (B,D) Projection of relative stiffness (from A,C) on measured leaf topography for WT (B) and *spy-3* (D). (E) Quantification of relative stiffness cell walls of the tooth (T) and the sinus (S). Each point represents a measured pixel. (F) Apparent Young's modulus (Pa) measured on transversal cell walls of WT teeth (n=11) and sinuses (n=11) and *spy-3* teeth (n=7) and sinuses (n=7). **P<0.01, ***P<0.001 (one-tailed unpaired Student's t-test).

SPY is a component of the boundary domain network

Here, we have shown that *spy* mutants display boundary domain defects during leaf development, resulting in leaves with reduced serrations. Leaf development is a complex and integrated process, which results from both global and local changes throughout developmental time. Therefore, we cannot rule out the possibility that the local changes we observed in the *spy-3* mutant may result from growth rate changes at the whole-organ level. Indeed, GA is involved in the proliferation/differentiation switch that occurs during leaf development. In *Arabidopsis*, DELLAs have been shown to increase the transcript levels of KIP-RELATED PROTEIN 2 (KRP2), SIAMESE (SIM) and SIM RELATED 1 and 2 (SMR1 and SMR2), which are all involved in inhibition of cell cycle progression (Achard et al., 2009). SPY has been shown to activate RGA (Zentella et al., 2017), and in *spy* mutants, cell cycle progression is less restricted, triggering a faster differentiation of the leaf blade. In addition, *GA20ox1* overexpression results in increased levels of bioactive GA and the corresponding lines display large leaves with more and larger cells (Gonzalez et al., 2010). Together, these results suggest that GA levels control both cell expansion and cell proliferation in leaves. In addition to its role in GA signaling repression, former studies indicated that SPY has a role in CK signaling promotion (Greenboim-Wainberg et al., 2005; Steiner et al., 2012). However, it was shown that CK promotes cell proliferation and that reduced CK levels lead to a decrease in cell divisions and consequently to smaller organs (Holst et al., 2011). Moreover, a recent study revealed that a CK/GA balance is responsible for leaf complexity in tomato plants as it controls the morphogenesis/differentiation switch (Israeli et al., 2021). Hence, it is also possible that CK signaling is partially impaired in the *spy-3*

Development (2022) 149, dev200359. doi:10.1242/dev.200359

mutant and, as a consequence, modifies the serration growth dynamics. Although we cannot exclude the possibility that SPY impacts global leaf development in multiple ways, we have seen that the *spy-3* mutation results in local changes in cell size, which indicate a SPY function in boundary definition. Accordingly, SPY acts redundantly with CUC2 and CUC3 to promote cotyledon separation, which is a developmental process in which cell expansion and cell division mostly do not occur simultaneously.

It is also important to note that, although SPY and CUCs are commonly expressed within leaf boundary domain cells, SPY expression in not restricted to these domains. This observation suggests that sinus-localized defects in the *spy-3* mutant may reflect different activity of SPY depending on the tissue where it is expressed and/or the possibility that leaf cells do not respond uniformly to SPY activity alterations.

SPY and CUC2 act through a common cell wall-related molecular network

At the organ level, the origin of serrations has long been debated (Bilsborough et al., 2011; Kawamura et al., 2010; Nikovics et al., 2006). Recently, morphometrics was used to reconstruct leaf developmental growth trajectories of the WT and *cuc2-1* loss-of-function mutants, which do not initiate serrations (Biot et al., 2016). This work shows that local growth repression arises first at the sinus of young WT leaf primordia, where CUC2 is expressed, then, subsequently, outgrowth appears at a distance. As neither growth repression nor teeth initiation was observed in the *cuc2-1* mutant, it was concluded that CUC2 is a key regulator for the coordination of cellular processes leading to the development of serrations. Our work provides a molecular framework for the growth repression function of CUC2. Indeed, we present evidence that CUC2 and SPY downregulate a set of common genes involved in cell wall loosening. Accordingly, we demonstrate that CUC2 inhibits cell elongation and that this cellular mode of action is accompanied with downregulation of transcripts encoding expansin-like and xyloglucan endotransglucosylases/hydrolases, which have been reported to be sufficient to promote hypocotyl cell elongation when overexpressed (Boron et al., 2015; Miedes et al., 2013). Unfortunately, no growth phenotypes have been reported for loss-of-function mutants for these genes, probably because of the high level of redundancy or the deleterious effects of multiple pleiotropic mutations.

Additionally, we demonstrate here that CUC2 can inhibit cell expansion independently of CUC3. Our current model for CUC2 activity states that *CUC2* is expressed early during leaf development and triggers serration development through CUC3 and KLUH, which act as molecular relays (Maugarny-Calès et al., 2019). Accordingly, CUC3 has been shown to inhibit cell expansion of sinus cells, hence contributing to shaping of the leaf (Serra and Perrot-rechenmann, 2020). Here, we completed this model by adding another route for the growth repression of sinus cells. As CUC2 can regulate cell expansion independently of CUC3, it is probable that CUC2 contributes also to the local growth repression process per se. This reveals an entangled role for CUC2 in coordinating patterning and cell growth to define boundary domains.

Cell wall mechanics at the leaf margin

Our data show that sinuses and teeth display differential cell wall stiffness even at early stages of leaf development. This differential stiffness is reduced in the *spy-3* mutant, in which sinus cell walls resemble teeth cell walls. Here, the *spy-3* mutant allows us to differentiate CUC2 functions as SPY and CUC2 act on a common molecular network related to cell wall loosening. Our work reveals the contribution of cell wall mechanics to morphogenesis: local cell wall parameters will greatly impinge on the growth of the whole organ. Moreover, CUC3 has been shown to act downstream of CUC2 (Maugarny-Calès et al., 2019), and its expression is promoted by mechanical stresses (Fal et al., 2016). It is therefore tempting to propose a model in which CUC2 activity induces mechanical stress at the margins, which could then trigger CUC3 expression to serve as a relay for local growth repression. Further experiments will be needed to provide a comprehensive view of the integration of hormonal, genetic and mechanical stress in leaf development and boundary domain development in general.

MATERIALS AND METHODS

Plant material and growth conditions

All plants used in this study were in the Columbia (Col-0) background except the *cuc2-1* mutant which was originally obtained in the Landsberg (Ler-0) background and back-crossed five times to Col-0. For morphometric analysis, seeds were immersed in distilled water for 2 days in the dark at 4°C before sowing on soil. Then, plants were grown under short-day conditions [6 h day (21°C, hygrometry 65%, light 120 µM/m^2/s), 1 h dusk (21°C, hygrometry 65%, light 80 µM/m^2/s), 16 h night (18°C, hygrometry 65%, dark conditions), 1 h dawn (19°C, hygrometry 65%, light 80 µM/m^2/s)]. For *in vitro* cultures, seeds were sown on *Arabidopsis* medium (Gonçalves et al., 2017), stratified for 48 h in the dark at 4°C then transferred to long-day conditions (21°C, 16 h day/8 h night, light 50 µM/m^2/s).

Morphometric analysis

For morphometric analysis of mature leaves, leaves from ranks 11, 12 and 13 from 6-week-old plants were harvested and glued on a paper sheet prior to scanning using a Perfection V800 Photo scanner (Epson) at 1600 dpi. For morphometric analysis of developing leaves, young leaf primordia (ranks 11, 12 and 13) were dissected using a stereomicroscope throughout development starting at day 22 after sowing. Leaves were mounted between a slide and a coverslip in a buffer containing 10 mM Tris HCl, pH 8.5, and 0.01% (v/v) Triton X-100 and imaged using an Axio Zoom.V16 microscope (Carl Zeiss Microscopy). Depending on the developmental stage imaged, either the chlorophyll fluorescent signal or the brightfield signal were collected. Leaf silhouettes and measurements were obtained using MorphoLeaf software, which allows semi-automatic leaf segmentation and the extraction of relevant biological parameters (Biot et al., 2016). Output data analysis, statistics and plots were generated using R software (http://www.R-project.org/) and the graphics package ggplot2. For all boxplots, the lower box limit represents the 25th percentile (Q1) and the upper box limit represents the 75th percentile (Q3); the median (Q2) is represented by the centre line; whiskers indicate the minimum and maximum values in the data [respectively, Q1-1.5*interquartile range (IQR) and Q3+1.5*IQR].

Confocal imaging

For quantification of cellular parameters, we used the *pPDF1::mCitrine-KA1* line (Stanislas et al., 2018) in order to visualize the plasma membrane in the leaf epidermis. Col-0 and *spy-3* plants (26-31 days old) containing the *pPDF1::mCitrine-KA1* construct were grown under short-day conditions prior to dissecting, mounting in a buffer containing 10 mM Tris HCl, pH 8.5, and 0.01% (v/v) Triton X-100 and direct imaging with a Leica SP5 inverted microscope (Leica Microsystems). Samples were excited using a 514 nm laser and fluorescence was collected with a hybrid detector at between 569 and 611 nm. TIF images were rotated using the TransformJ plugin of ImageJ. Subsequent cell segmentations, cell curvature and cell surface area measurements were then obtained using MorphoGraphX (MGX) (de Reuille et al., 2015) software (http://www.mpipz.mpg.de/MorphoGraphX/). Cells corresponding to tooth sinus were identified as cells displaying a fully negative signal when projecting a 15 µm-neighboring Gaussian curvature (Serra and Perrot-rechenmann, 2020). The *pSPY::SPY-GFP*, *pCUC3::CFP* and *pCUC2::RFP* reporter lines were imaged with a Leica SP5 inverted microscope (Leica Microsystems). GFP was excited

Development (2022) 149, dev200359. doi:10.1242/dev.200359

using a 488 nm laser and fluorescence was collected with a hybrid detector at between 500 and 530 nm. RFP was excited at 561 nm and detected with a PMT detector within 570 and 635 nm. CFP was excited at 458 nm and detected with a PMT detector within 460 and 475 nm.

Transcriptomic analysis

RNA samples

For RNA-seq assays, *p35S:CUC2-GR* seedlings were grown in liquid *Arabidopsis* medium with constant shaking. After 10 days of growth under constant light, seedlings were treated with DEX or mock solution for 6 h and then snap-frozen in liquid nitrogen. DEX (Sigma-Aldrich, D1756) was dissolved in 100% ethanol and used at a final concentration of 10 µM. Total RNA extraction was performed with the *mir*Vana extraction kit (Ambion) following the manufacturer's recommendations.

Leaf margins from WT and the *CUC2g-m4* line grown for 3 weeks in short-day conditions were microdissected in triplicate with the ZEISS PALM MicroBeam using a Fluar 5×/0.25 M27 objective. Young leaves (≈1-2 mm long) from ranks 6 and 7 were dissected, placed onto MMI membrane slides and microdissected leaf margins (defined as proximal teeth without differentiated trichomes) were collected in Zeiss adhesive caps. For every biological replicate, approximately ten leaf margins were collected. Total RNA extraction was performed using the Arcturus PicoPure RNA Isolation Kit (Thermo Fisher Scientific), following the manufacturer's instructions and RNA quality was controlled using the Agilent RNA 6000 Pico Kit.

RNA-seq libraries

RNA-seq libraries were constructed by the POPS platform (IPS2) using the TruSeq non-stranded mRNA library prep kit (Illumina) according to the supplier's instructions. The libraries were sequenced in paired-end reads (PE, 2×100 bases) on an Illumina HiSeq 2000 to generate a mean of 30 million of PE reads per sample. A quality control process removed PE reads with Qscore<20, length<30 bases and ribosomal reads.

Bioinformatic analyses

Filtered PE reads were mapped using Bowtie 2 (Langmead and Salzberg, 2012) with the –local option against the *Arabidopsis thaliana* transcriptome. The 33,602 genes were extracted from TAIR v10 database; 95% of PE reads were associated with one gene unambiguously, 2% were removed for multi-hits. Genes with <1 read per million in at least half of the samples were discarded. The resulting raw count matrix was fed into edgeR (Robinson et al., 2010) for differential expression testing by fitting a negative binomial generalized log-linear model (GLM) including a condition factor and a replicate factor to the TMM-normalized read counts for each gene. We performed pairwise comparisons of each of the DEX-treated condition to the control condition. The distribution of the resulting *P*-values followed the quality criterion described by Rigaill et al. (2018). Genes with an adjusted *P*-value (FDR, Benjamini–Hochberg adjustment) below 0.05 were considered as differentially expressed.

Dark-grown hypocotyl measurements

For dark-grown hypocotyl experiments, seeds were surface-sterilized and subsequently dispatched on 1% agar (w/v) *Arabidopsis* media with 10 µM DEX (Sigma-Aldrich, D1756) or mock treatment. After 48 h in the dark at 4°C, plates were transferred to a growth chamber for 6 h (21°C, light 50 µM/m^2/s) before being placed vertically in the dark at 21°C. Plates were scanned after 72 h of dark growth using a Perfection V800 Photo scanner (Epson) at 1600 dpi. Hypocotyl sizes were measured using the NeuronJ plugin from Fiji and data were analyzed using R software (http://www.R-project.org/).

Expression data

Total RNA was isolated using the RNeasy Plant Mini Kit (QIAGEN) following the manufacturer's recommendation for plant tissue. Reverse transcription was performed using RevertAid H Minus M-MuLV Reverse transcriptase (Fermentas/Thermo Fisher Scientific) followed by a RNase H treatment was performed for 20 min 37°C to eliminate DNA-RNA duplexes. Real-time PCR analysis was performed on a 384-well QuantStudio™ 5 Real-Time PCR System, using the SsoAdvanced Universal SYBR Green Supermix with the following PCR conditions: 95°C 3 min; (95°C 15 s; 63°C 30 s)×40 cycles. Raw data were analyzed using QuantStudio Design and Analysis software v2.2. Primers used for real-time PCR analysis are available in Table S2. Expression data were normalized using the ΔΔCt method using at least two independent reference genes.

AFM

For mechanical characterization of the leaf cell wall, WT and *spy-3* plants were grown on soil in short-day conditions. About 100- to 200 µm-long young leaf primordia from rank higher than 11 were hand-dissected under a stereomicroscope and collected. For mechanical characterization of dark-grown hypocotyl cell wall of plants overexpressing CUC2, 48-h-old seedlings from the *p35S:CUC2-GR* line and WT grown in the dark on 1 µM DEX were collected. Samples were fixed in low melting agarose with blade facing the AFM tip following the protocol described by Peaucelle (2014). Samples were plasmolysed by immersion in 10% (m/v) sorbitol. An AFM cantilever loaded with a 1 µm diameter tip was used in these measurements and scanned 100 µm×30 µm areas with a fixed force leading to a maximum indentation value of 800 nm with a speed of 40 μms^{-1}. The measurement of the rigidity constant was performed only on the second cantiliever used as a reference tip as described by Peaucelle (2014). The relative stiffness was used as a proxy of cell wall stiffness, which is relative to the rigidity constant of the cantilever used. Apparent Young's modulus was determined by a Hertzian indentation model on each indentation point. Cell topography was reconstructed using the height at each point of contact. Data were analyzed and maps were plotted using MATLAB.

Acknowledgements

We thank Utpal Nath (Indian Institute of Science Bangalore) for the gift of *spy-3* seeds; Doris Lucyshyn (BOKU, Vienna, Austria) for sharing with us the *spy-22* and *spy-23* mutants, the pSPY::SPY-FLAG spy-22 and the pSPY::SPY-GFP lines; and Ben Scheres (Wageningen University, the Netherlands) for the gift of the p35S: CUC2-GR line. We thank Genoscope - Centre National de Séquençage (Evry, France) for allowing us privileged access to perform sequencing. We thank Antoine Nicolas for discussions and critical reading of the manuscript. The IJPB benefits from the support of the Labex Saclay Plant Sciences-SPS (ANR-10-LABX-0040-SPS).

Competing interests

The authors declare no competing or financial interests.

Author contributions

Conceptualization: N. Bouré, P.L., N.A.; Methodology: N. Borrega; Software: E.B.; Formal analysis: N. Bouré, A.P., Z.T., M.-L.M.-M., N.A.; Investigation: N. Bouré, A.P., M.G., B.A., L.S.-T., V.P., N.A.; Writing - original draft: N. Bouré, P.L., N.A.; Visualization: N. Bouré, N.A.; Supervision: N.A.; Project administration: N.A.; Funding acquisition: N.A., V.P.

Funding

This work was supported by the Agence National de la Recherche grants LEAFNET (ANR-12-PDOC-0003) and CHARMFUL (ANR-11-BSV2-0005) and by an Institut National de Recherche pour l'Agriculture, l'Alimentation et l'Environnement (INRAE) grant MorphEAT (AAP BAP 2020).

Data availability

RNA-seq data have been deposited in the Gene Expression Omnibus database under accession number GSE184530. All steps of the experiment, from growth conditions to bioinformatic analyses, are detailed in POPS database, CATdb (Gagnot et al., 2008; http://tools.ips2.u-psud.fr/CATdb/project.html?project_id=491).

Peer review history

The peer review history is available online at https://journals.biologists.com/dev/article-lookup/doi/10.1242/dev.200359.

References

Achard, P., Gusti, A., Cheminant, S., Alioua, M., Dhondt, S., Coppens, F., Beemster, G. T. S. and Genschik, P. (2009). Gibberellin signaling controls cell proliferation rate in Arabidopsis. *Curr. Biol.* **19**, 1188-1193. doi:10.1016/j.cub.2009.05.059

Aida, M. and Tasaka, M. (2006). Morphogenesis and patterning at the organ boundaries in the higher plant shoot apex. *Plant Mol. Biol.* **60**, 915-928. doi:10.1007/s11103-005-2760-7

Aida, M., Ishida, T., Fukaki, H., Fujisawa, H. and Tasaka, M. (1997). Genes involved in organ separation in Arabidopsis: an analysis of the cup-shaped cotyledon mutant. *Plant Cell* **9**, 841-857. doi:10.1105/tpc.9.6.841

Aida, M., Ishida, T. and Tasaka, M. (1999). Shoot apical meristem and cotyledon formation during Arabidopsis embryogenesis: interaction among the CUP-SHAPED COTYLEDON and SHOOT MERISTEMLESS genes. *Development* **126**, 1563-1570. doi:10.1242/dev.126.8.1563

Bell, E. M., Lin, W., Husbands, A. Y., Yu, L., Jaganatha, V., Jablonska, B., Mangeon, A., Neff, M. M., Girke, T. and Springer, P. S. (2012). Arabidopsis LATERAL ORGAN BOUNDARIES negatively regulates brassinosteroid accumulation to limit growth in organ boundaries. *Proc. Natl. Acad. Sci. USA* **109**, 21146-21151. doi:10.1073/pnas.1210789109

Bilsborough, G. G. D., Runions, A., Barkoulas, M., Jenkins, H. W., Hasson, A., Galinha, C., Laufs, P., Hay, A., Prusinkiewicz, P. and Tsiantis, M. (2011). Model for the regulation of Arabidopsis thaliana leaf margin development. *Proc. Natl. Acad. Sci. USA* **108**, 3424-3429. doi:10.1073/pnas.1015162108

Biot, E., Cortizo, M., Burguet, J., Kiss, A., Oughou, M., Maugarny-Calès, A., Gonçalves, B., Adroher, B., Andrey, P., Boudaoud, A. et al. (2016). Multiscale quantification of morphodynamics: MorphoLeaf software for 2D shape analysis. *Development* **143**, 3417-3428. doi:10.1242/dev.134619

Blein, T., Pulido, A., Vialette-Guiraud, A., Nikovics, K., Morin, H., Hay, A., Johansen, I. E., Tsiantis, M. and Laufs, P. (2008). A conserved molecular framework for compound leaf development. *Science* **322**, 1835-1839. doi:10.1126/science.1166168

Boron, A. K., van Loock, B., Suslov, D., Markakis, M. N., Verbelen, J.-P. and Vissenberg, K. (2015). Over-expression of AtEXLA2 alters etiolated arabidopsis hypocotyl growth. *Ann. Bot.* **115**, 67-80. doi:10.1093/aob/mcu221

Burian, A., Raczyńska-Szajgin, M., Borowska-Wykręt, D., Piatek, A., Aida, M. and Kwiatkowska, D. (2015). The CUP-SHAPED COTYLEDON2 and 3 genes have a post-meristematic effect on Arabidopsis thaliana phyllotaxis. *Ann. Bot.* **115**, 807-820. doi:10.1093/aob/mcv013

Dahmann, C., Oates, A. C. and Brand, M. (2011). Boundary formation and maintenance in tissue development. *Nat. Rev. Genet.* **12**, 43-55. doi:10.1038/nrg2902

de Reuille, P. B., Routier-Kierzkowska, A.-L., Kierzkowski, D., Bassel, G. W., Schüpbach, T., Tauriello, G., Bajpai, N., Strauss, S., Weber, A., Kiss, A. et al. (2015). MorphoGraphX: a platform for quantifying morphogenesis in 4D. *eLife* **4**, e05864. doi:10.7554/eLife.05864

Fal, K., Landrein, B. and Hamant, O. (2016). Interplay between miRNA regulation and mechanical stress for CUC gene expression at the shoot apical meristem. *Plant Signal. Behav.* **11**, e1127497. doi:10.1080/15592324.2015.1127497

Gagnot, S., Tamby, J.-P., Martin-Magniette, M.-L., Bitton, F., Taconnat, L., Balzergue, S., Aubourg, S., Renou, J.-P., Lecharny, A. and And Brunaud, V. (2008). CATdb: a public access to Arabidopsis transcriptome data from the URGV-CATMA platform. *Nucleic Acids Res.* **36**, D986-D990. doi:10.1093/nar/gkm757

Gendreau, E., Traas, J., Desnos, T., Grandjean, O., Caboche, M. and Höfte, H. (1997). Cellular basis of hypocotyl growth in Arabidopsis thaliana. *Plant Physiol.* **114**, 295-305. doi:10.1104/pp.114.1.295

Gendron, J. M., Liu, J.-S., Fan, M., Bai, M.-Y., Wenkel, S., Springer, P. S., Barton, M. K. and Wang, Z.-Y. (2012). Brassinosteroids regulate organ boundary formation in the shoot apical meristem of Arabidopsis. *Proc. Natl. Acad. Sci. USA* **109**, 21152-21157. doi:10.1073/pnas.1210799110

Gonçalves, B., Hasson, A., Belcram, K., Cortizo, M., Morin, H., Nikovics, K., Vialette-Guiraud, A., Takeda, S., Aida, M., Laufs, P. et al. (2015). A conserved role for CUP-SHAPED COTYLEDON genes during ovule development. *Plant J.* **83**, 732-742. doi:10.1111/tpj.12923

Gonçalves, B., Maugarny-Calès, A., Adroher, B., Cortizo, M., Borrega, N., Blein, T., Hasson, A., Gineau, E., Mouille, G., Laufs, P. et al. (2017). GDP-L-fucose is required for boundary definition in plants. *J. Exp. Bot.* **68**, 5801-5811. doi:10.1093/jxb/erx402

Gonzalez, N., De Bodt, S., Sulpice, R., Jikumaru, Y., Chae, E., Dhondt, S., Van Daele, T., De Milde, L., Weigel, D., Kamiya, Y. et al. (2010). Increased leaf size: different means to an end. *Plant Physiol.* **153**, 1261-1279. doi:10.1104/pp.110.156018

Greenboim-Wainberg, Y., Maymon, I., Borochov, R., Alvarez, J., Olszewski, N. and Ori, N. (2005). Cross talk between Gibberellin and Cytokinin : the arabidopsis GA response inhibitor SPINDLY plays a positive role in cytokinin signaling. *Plant Cell* **17**, 92-102. doi:10.1105/tpc.104.028472

Hasson, A., Plessis, A., Blein, T., Adroher, B., Grigg, S., Tsiantis, M., Boudaoud, A., Damerval, C. and Laufs, P. (2011). Evolution and diverse roles of the CUP-SHAPED COTYLEDON genes in Arabidopsis leaf development. *Plant Cell* **23**, 54-68. doi:10.1105/tpc.110.081448

Hay, A., Kaur, H., Phillips, A., Hedden, P., Hake, S. and Tsiantis, M. (2002). The gibberellin pathway mediates KNOTTED1-type homeobox function in plants with different body plans. *Curr. Biol.* **12**, 1557-1565. doi:10.1016/S0960-9822(02)01125-9

Hepworth, S. R. and Pautot, V. A. (2015). Beyond the divide: boundaries for patterning and stem cell regulation in plants. *Front. Plant Sci.* **6**, 1052. doi:10.3389/fpls.2015.01052

Holst, K., Schmülling, T. and Werner, T. (2011). Enhanced cytokinin degradation in leaf primordia of transgenic Arabidopsis plants reduces leaf size and shoot organ primordia formation. *J. Plant Physiol.* **168**, 1328-1334. doi:10.1016/j.jplph.2011.03.003

Irvine, K. D. and Rauskolb, C. (2001). Boundaries in development: formation and function. *Annu. Rev. Cell Dev. Biol.* **17**, 189-214. doi:10.1146/annurev.cellbio.17.1.189

Israeli, A., Burko, Y., Shleizer-Burko, S., Zelnik, I. D., Sela, N., Hajirezaei, M. R., Fernie, A. R., Tohge, T., Ori, N. and Bar, M. (2021). Coordinating the morphogenesis- differentiation balance by tweaking the cytokinin-gibberellin equilibrium. *PLoS Genet.* **17**, e1009537. doi:10.1371/journal.pgen.1009537

Jacobsen, S. E. and Olszewski, N. E. (1993). Mutations at the SPINDLY locus of Arabidopsis alter gibberellin signal transduction. *Plant Cell* **5**, 887-896. doi:10.1105/tpc.5.8.887

Jacobsen, S. E., Binkowski, K. A. and Olszewski, N. E. (1996). SPINDLY, a tetratricopeptide repeat protein involved in gibberellin signal transduction in Arabidopsis. *Proc. Natl. Acad. Sci. USA* **93**, 9292-9296. doi:10.1073/pnas.93.17.9292

Jasinski, S., Piazza, P., Craft, J., Hay, A., Woolley, L., Rieu, I., Phillips, A., Hedden, P. and Tsiantis, M. (2005). KNOX action in arabidopsis is mediated by coordinate regulation of cytokinin and Gibberellin activities. *Curr. Biol.* **15**, 1560-1565. doi:10.1016/j.cub.2005.07.023

Kawamoto, N., Del Carpio, D. P., Hofmann, A., Mizuta, Y., Kurihara, D., Higashiyama, T., Uchida, N., Torii, K. U., Colombo, L., Groth, G. et al. (2020). A peptide pair coordinates regular ovule initiation patterns with seed number and fruit size. *Curr. Biol.* **30**, 4352-4361. doi:10.1016/j.cub.2020.08.050

Kawamura, E., Horiguchi, G. and Tsukaya, H. (2010). Mechanisms of leaf tooth formation in Arabidopsis. *Plant J.* **1**, 429-441. doi:10.1111/j.1365-313X.2010.04156.x

Kohnen, M. V., Schmid-Siegert, E., Trevisan, M., Petrolati, L. A., Sénéchal, F., Müller-Moulé, P., Maloof, J., Xenarios, I. and Fankhauser, C. (2016). Neighbor detection induces organ-specific transcriptomes, revealing patterns underlying hypocotyl-specific growth. *Plant Cell* **28**, 2889-2904. doi:10.1105/tpc.16.00463

Kosentka, P. Z., Overholt, A., Maradiaga, R., Mitoubsi, O. and Shpak, E. D. (2019). EPFL signals in the boundary region of the SAM restrict its size and promote leaf initiation. *Plant Physiol.* **179**, 265-279. doi:10.1104/pp.18.00714

Langmead, B. and Salzberg, S. L. (2012). Fast gapped-read alignment with Bowtie 2. *Nat. Methods* **9**, 357-359. doi:10.1038/nmeth.1923

Laufs, P., Peaucelle, A., Morin, H. and Traas, J. (2004). MicroRNA regulation of the CUC genes is required for boundary size control in Arabidopsis meristems. *Development* **131**, 4311-4322. doi:10.1242/dev.01320

Maugarny-Calès, A., Cortizo, M., Adroher, B., Borrega, N., Gonçalves, B., Brunoud, G., Vernoux, T., Arnaud, N. and Laufs, P. (2019). Dissecting the pathways coordinating patterning and growth by plant boundary domains. *PLoS Genet.* **15**, e1007913. doi:10.1371/journal.pgen.1007913

Maymon, I., Greenboim-wainberg, Y., Sagiv, S., Kieber, J. J., Moshelion, M., Olszewski, N. and Weiss, D. (2009). Cytosolic activity of SPINDLY implies the existence of a DELLA-independent gibberellin-response pathway. *Plant J.* **58**, 979-988. doi:10.1111/j.1365-313X.2009.03840.x

Miedes, E., Suslov, D., Vandenbussche, F., Kenobi, K., Ivakov, A., Van der Straeten, D., Lorences, E. P., Mellerowicz, E. J., Verbelen, J.-P. and Vissenberg, K. (2013). Xyloglucan endotransglucosylase/hydrolase (XTH) overexpression affects growth and cell wall mechanics in etiolated Arabidopsis hypocotyls. *J. Exp. Bot.* **64**, 2481-2497. doi:10.1093/jxb/ert107

Mutanwad, K. V., Zangl, I. and Lucyshyn, D. (2020). The Arabidopsis O-fucosyltransferase SPINDLY regulates root hair patterning independently of gibberellin signaling. *Development* **147**, dev192039. doi:10.1242/dev.192039

Nikovics, K., Blein, T., Peaucelle, A., Ishida, T., Morin, H., Aida, M. and Laufs, P. (2006). The balance between the MIR164A and CUC2 genes controls leaf margin serration in Arabidopsis. *Plant Cell* **18**, 2929-2945. doi:10.1105/tpc.106.045617

O'Neill, M. A., Eberhard, S., Albersheim, P. and Darvill, A. G. (2001). Requirement of borate cross-linking of cell wall rhamnogalacturonan II for Arabidopsis growth. *Science* **294**, 846-849. doi:10.1126/science.1062319

Peaucelle, A. (2014). AFM-based mapping of the elastic properties of cell walls: at tissue, cellular, and subcellular resolutions. *J. Vis. Exp.* **89**, e51317. doi:10.3791/51317

Qin, F., Kodaira, K.-S., Maruyama, K., Mizoi, J., Tran, L.-S. P., Fujita, Y., Morimoto, K., Shinozaki, K. and Yamaguchi-Shinozaki, K. (2020). SPINDLY, a negative regulator of gibberellic acid signaling, is involved in the plant abiotic. *Plant Physiol.* **157**, 1900-1913. doi:10.1104/pp.111.187302

Rigaill, G., Balzergue, S., Brunaud, V., Blondet, E., Rau, A., Rogier, O., Caius, J., Maugis-Rabusseau, C., Soubigou-Taconnat, L., Aubourg, S. et al. (2018). Synthetic data sets for the identification of key ingredients for RNA-seq differential analysis. *Brief. Bioinform.* **19**, 65-76.

Robinson, M. D., McCarthy, D. J. and Smyth, G. K. (2010). edgeR: a Bioconductor package for differential expression analysis of digital gene expression data. *Bioinformatics* **26**, 139-140. doi:10.1093/bioinformatics/btp616

Serra, L. and Perrot-rechenmann, C. (2020). Spatiotemporal control of cell growth by CUC3 shapes leaf margins. *Development* **147**, dev183277. doi:10.1242/dev.183277

Stanislas, T., Platre, M. P., Liu, M., Rambaud-lavigne, L. E. S., Jaillais, Y. and Hamant, O. (2018). A phosphoinositide map at the shoot apical meristem in Arabidopsis thaliana. *BMC Biol.* **16**, 20. doi:10.1186/s12915-018-0490-y

Steiner, E., Efroni, I., Gopalraj, M., Saathoff, K., Tseng, T.-S., Kieffer, M., Eshed, Y., Olszewski, N. and Weiss, D. (2012). The arabidopsis O -linked N-acetylglucosamine transferase SPINDLY interacts with class I TCPs to facilitate cytokinin responses in leaves and flowers. *Plant Cell* **24**, 96-108. doi:10.1105/tpc.111.093518

Strasser, R. (2016). Plant protein glycosylation. *Glycobiology* **26**, 926-939. doi:10.1093/glycob/cww023

Swain, S. M., Tseng, T.-S. and Olszewski, N. E. (2001). Altered expression of SPINDLY affects gibberellin response and plant development 1. *Plant Physiol.* **126**, 1174-1185. doi:10.1104/pp.126.3.1174

Tameshige, T., Okamoto, S., Lee, J. S., Aida, M., Tasaka, M., Torii, K. U. and Uchida, N. (2016). A secreted peptide and its receptors shape the auxin response pattern and leaf margin morphogenesis. *Curr. Biol.* **26**, 2478-2485. doi:10.1016/j.cub.2016.07.014

Van Hengel, A. J. and Roberts, K. (2002). Fucosylated arabinogalactan-proteins are required for full root cell elongation in arabidopsis. *Plant J.* **32**, 105-113. doi:10.1046/j.1365-313X.2002.01406.x

Vroemen, C. W., Mordhorst, A. P., Albrecht, C., Kwaaitaal, M. A. C. J. and de Vries, S. C. (2003). The CUP-SHAPED COTYLEDON3 gene is required for boundary and shoot meristem formation in arabidopsis. *Plant Cell* **15**, 1563-1577. doi:10.1105/tpc.012203

Wang, Y., He, Y., Su, C., Zentella, R., Sun, T. and Wang, L. (2020). Nuclear Localized O -Fucosyltransferase SPY facilitates PRR5 proteolysis to fine-tune the pace of arabidopsis circadian clock. *Mol. Plant* **13**, 446-458. doi:10.1016/j.molp.2019.12.013

Zentella, R., Sui, N., Barnhill, B., Hsieh, W.-P., Hu, J., Shabanowitz, J., Boyce, M., Olszewski, N. E., Zhou, P., Hunt, D. F. et al. (2017). The arabidopsis O-fucosyltransferase SPINDLY activates nuclear growth repressor DELLA. *Nat. Chem. Biol.* **13**, 479-485. doi:10.1038/nchembio.2320